Journal of Materials Chemistry A

PAPER

View Article Online
View Journal | View Issue

Cite this: J. Mater. Chem. A, 2014, 2, 3175

Highly efficient flexible cathodes for dye sensitized solar cells to complement Pt@TCO coatings

Jesus Idígoras,[b] Elena Guillén,[a] F. Javier Ramos,[a] Juan A. Anta,[b] Mohammad K. Nazeeruddin[c] and Shahzada Ahmad*[a]

Received 4th September 2013
Accepted 24th November 2013

DOI: 10.1039/c3ta13524a

www.rsc.org/MaterialsA

Solution-processed, semi-transparent, conductive electrodes based on PEDOT:PSS [poly(3,4-ethylenedioxythiophene):poly(styrenesulfonate)] using silver grids were developed on a plastic support. The flexible electrode (flextrode) was employed as a cathode in dye sensitized solar cells (DSSCs) and acts in two-fold manner: the PEDOT layer will yield a high surface area for effective electrocatalysis, while the silver grid will decrease the series resistance to rival transparent conducting oxide (TCO) coatings. DSSCs fabricated with **Y123** dye and the developed cathodes show power conversion efficiencies of 7%, which are comparable to the reference device (6.9%) using Pt@FTO (F-doped SnO_2) coatings on glass under the same conditions. A flexible and cost effective electrode will help to penetrate the market for DSSCs and hybrid-organic–inorganic photovoltaics. Electrochemical impedance spectroscopy and modelling results confirm similar values of the series resistance and charge transfer resistance of the cathodes both in Pt-based and PEDOT-based cells, as well as the limited impact on the *I–V* curve from the modification of the charge transfer parameters in the PEDOT-based cells.

1. Introduction

Clean sources of energy are needed by modern society and can be achieved by renewable resources, especially the conversion of solar energy into electricity.[1] Among the numerous photovoltaic (PV) technologies currently available, emerging (third generation) technologies have the potential to bring down the cost. In this scenario, dye-sensitized solar cells (DSSCs), or Grätzel cells, are one of the alternatives, ready to penetrate into the market owing to their low-cost fabrication processes and aesthetic benefits.[2–4] DSSCs can be fabricated as flexible devices for building integrated PV (BIPV) and work efficiently under diffuse light conditions. A DSSC is composed of a mesoporous network of wide band gap materials (TiO_2 nanoparticles) on which a monolayer of dye is tethered (photoanode), while the platinized cathode is separated by a redox shuttle (Fig. 1). The development of new sensitizers, semiconductor anodes and redox shuttles to obtain efficient devices is a matter of intense investigation.[4–7] However, due emphasis has not been given to finding alternate current collectors and for the reduction of redox shuttle used. Carbon-based low-cost materials are the front runner to replace the conventional Pt-based catalysts that constitute the counter-electrodes in DSSCs. Currently transparent conducting oxide (TCO) coated glasses are being used as charge collectors in DSSCs and they consume a large share of the cost in device fabrication.[8,9] The calculated cost of TCO in DSSCs is high (US $8–12 m^{-2} on the Gigawatt scale) and

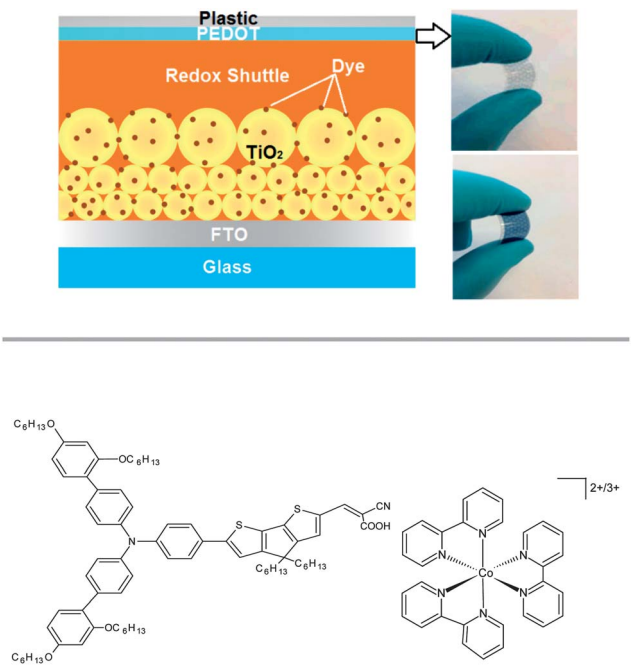

Fig. 1 Schematic diagram of DSSCs, flexible cathode with and without additional spin-coated PEDOT. Molecular structure of dye **Y123** and the cobalt trisbipyridine (bpy) complex used as the redox shuttle.

[a]Abengoa Research, C/Energía Solar no. 1, Campus Palmas Altas-41014, Sevilla, Spain. E-mail: shahzada.ahmad@research.abengoa.com

[b]Department of Physical, Chemical and Natural Systems, Universidad Pablo de Olavide, Sevilla 41013, Spain

[c]Department of Chemistry and Chemical Engineering, Swiss Federal Institute of Technology, Station 6, CH-1015 Lausanne, Switzerland

thus its replacement with cheaper, earth abundant alternatives would significantly reduce the cost per watt and energy payback time.[10] High cost, limited resources and high energy treatment during the TCO deposition process are some of the bottlenecks which require immediate alternatives.[10–12] More importantly in the case of flexible devices, the photoanode can be prepared on Ti foil, while the cathode still demands Pt@TCO coated substrates. Therefore, the search for alternative cathode materials continues and is paramount to bring down the cost of DSSCs in order to make them the undisputed choice for PV devices at a cost-effective price (< US \$20 m^{-2}).[8] The use of a Pt catalyst also has several drawbacks, such as high price (\$50 g^{-1}), low feed stocks and moderate stability caused by long-term exposure to the redox shuttle.[13,14] Thus it is vital to develop TCO and Pt free cathode materials that are cheaper but still capable of giving comparable photon to light conversion efficiency and device stability.[9,15] Graphene-based coatings have been exploited as a possible replacement for TCO glasses but they hardly match the requirements.[15] The unparalleled merit of poly(3,4-ethylenedioxythiophene) [PEDOT] is promising as a rival to TCO coatings. PEDOT has the merits of being less expensive, environmentally friendly in its processing and manufacturing, and has a low band gap (1.6 eV) and high conductivity with transmissive behaviour. The favourable ring geometry and its electron-donating ability make it stable under environmental conditions. In previous work, PEDOT-based cathodes were successfully demonstrated as an alternative for Pt catalysts.[14,16–18] *In situ* chemical polymerization of EDOT was performed on the glass and then used as a TCO replacement in DSSCs,[19] however these layers suffer from low adherence with the substrates. PEDOT alone cannot match the TCO replacement requirements and the obtained power conversion efficiency (PCE) with these current collectors are low. In this aspect, the synergistic effect of metal and PEDOT may prove to be beneficial,[20] and the strategy to increase the conductivity that can be employed is using the combination of silver (Ag) grid and poly(3,4-ethylenedioxythiophene)-poly(styrenesulfonate) PEDOT:PSS composite electrodes. This can dramatically reduce the per watt cost (the amount of Ag metal used in grid fabrication is negligible) and energy payback time of the fabricated devices. These flexible cathodes were fabricated using a reel-to-reel (R2R) mass production process and are considered to be a system of choice for large area integration in BIPV.[21,22] Such electrodes can drastically decrease the series resistance (R_s) from >1 kΩ in devices with only PEDOT:PSS as the electrode to 400 Ω for composite electrodes.[20] We have employed a R2R processed PEDOT flexible substrate on a pre-deposited honeycomb structured Ag grid (deposited by a R2R ink jet printer). To further lower the sheet resistance, an additional layer of PEDOT can be spin-coated on top of these flexible substrates.

The two electron process based redox shuttle triiodide/iodide (I_3^-/I^-) has been employed for over two decades, but it absorbs light and can dissolve Au and Ag catalysts. Additionally, it shows a low redox potential (0.35 V *versus* standard hydrogen electrode), which is unsuitable for regeneration of the dye, leading to loss in the regeneration process, the open-circuit potential (V_{oc}), and thus limits the PCE. A one electron based cobalt redox shuttle in the presence of an organic dye works efficiently and gives record V_{oc} values.[5,6,23] Furthermore, the use of a platinized cathode (Pt@TCO) is not optimal in the presence of a cobalt redox shuttle and here carbon-based catalysts outperform Pt. We demonstrate the fabrication of DSSCs by using flexible PEDOT cathodes with a metal grid and a cobalt-based redox shuttle, and their performance was compared to devices with the classical platinized cathode. A remarkable PCE of 7% was obtained, which not only matches the value of a standard DSSC (6.9%), but at the fraction of the cost with having additional advantage of being flexible, as well as processable at ambient temperature and environment. To understand the charge transport properties in these cathodes, electrochemical impedance spectroscopy (EIS) under illumination was used to analyse the performance of the fabricated cells.

2. Results and discussions

2.1 Electrochemical activity of PEDOT-based and platinized cathodes

The electrocatalytic properties of the platinized and PEDOT-based cathodes used in the device fabrication were compared with the help of cyclic voltammetry in a two-electrode configuration (blank cells, Fig. 2). Two types of blank cells were prepared: a Pt@FTO/Pt@FTO configuration (formed by two platinized cathodes) and a PEDOT/Pt@FTO configuration (formed by a platinized FTO and an electrode denoted as Cathode 2). Further details regarding the electrodes and cell setup can be found in the Experimental section. The ratio of the peak current densities, i_{pa}/i_{pc}, is close to unity in both these cases pointing towards excellent reversibility of these electrodes. The redox activity of the polymer films is hence reversible and yielded higher current densities (5.25 mA cm^{-2} anodic, 6.05 mA cm^{-2} for cathodic) than platinized cathodes (4.6 mA cm^{-2} anodic, 5.35 mA cm^{-2} for cathodic). The catalytic activity of the PEDOT-based cathode is slightly better than with a platinized cathode and no significant mass transfer limitation can be inferred. The improved electrocatalytic activity of the PEDOT cathode is mainly due to the high surface area of the

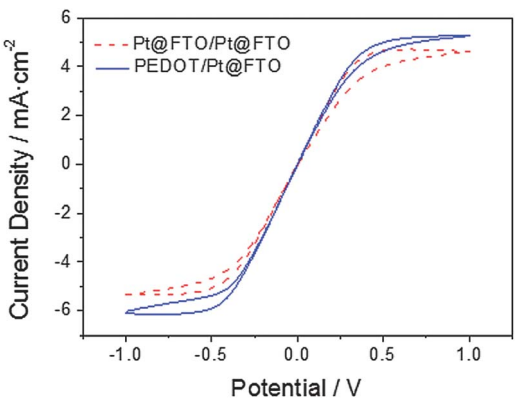

Fig. 2 Cyclic voltammetry of Pt@FTO/Pt@FTO and PEDOT/Pt@FTO blank cells.

PEDOT with respect to monocrystalline platinum.[27] We assume that the high surface area and porous morphology of the PEDOT will result in a fast reaction rate and will give low charge transfer resistance at the interface of the redox shuttle and cathode.

2.2 Photovoltaic performance of DSSCs

J–V curves (Fig. 3) for DSSCs based on Pt@FTO and Cathode 2 are shown. The DSSC sensitized by **Y123** with a cobalt redox shuttle using a PEDOT-based cathode (Cathode 2) gave a very promising PV performance, showing a short circuit photocurrent density (J_{sc}) of 13.4 mA cm^{-2}, V_{oc} of 790 mV and ~0.66 fill factor (FF) resulting in a PCE of 7% under standard global AM (Air Mass) 1.5 solar conditions. Under the same conditions, the PCE when using a platinized cathode was slightly lower or comparable (6.9%). The additional layer of PEDOT (Cathode 2) helped to reduce the series resistance and gave a higher J_{sc} than Cathode 1, which yielded a PCE of <5%. Table 1 summarizes the performance parameters of the most efficient cells along with the average and standard deviation values for a batch of 3 cells fabricated in a similar fashion.

The polymer-based cathodes showed a negligible ~10 mV difference in V_{oc} when compared to the platinized cathode. In the past we have observed a similar loss in V_{oc} when using PEDOT as an electrocatalyst on FTO substrates, which was ascribed to a charge transfer overpotential at the FTO/PEDOT interface or electrolyte/PEDOT and/or the electrical sheet resistance.[24]

It is worth mentioning here that the polymer cathodes yielded relatively higher FF values when compared to a previous report on a PEDOT cathode,[9] possibly due to the use of a Ag honeycombed structure (metal grids) on the flexible substrates. The incident photon-to-current efficiency (IPCE) as a function of wavelength reaches a maximum of 80% in most of the visible spectrum, which is comparable with the device with a platinized cathode (Fig. 4). The UV-vis spectrum of dye **Y123** in solution is also shown in Fig. 4. It should be noted that the IPCE spectrum is significantly broader than the spectrum of the isolated dye, which is well in accordance with the literature.

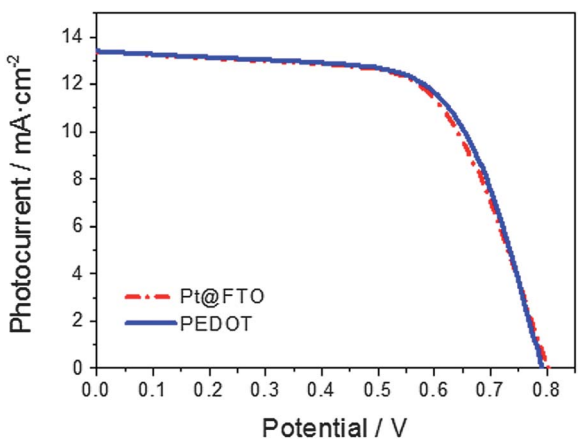

Fig. 3 *J–V* curves of platinized cathode and polymer-based flexible cathode.

2.3 EIS study of complete cells

EIS measurements were carried out in complete DSSCs based on Cathode 2 (PEDOT) or a Pt@FTO cathode. Nyquist plots (Fig. 5a) at an applied bias close to the V_{oc} at 1 sun (0.7 V) are shown for both types of cells. An enlargement of the high frequency region is shown in the inset. The spectra were fitted to the equivalent circuit showed in Fig. 5b. The different components in this circuit have the following physical meaning: R_s is the total series resistance of the cell, R_{rec} and C_μ are the recombination charge transfer resistance and the chemical capacitance at the oxide/electrolyte interface, R_{CE} and C_{CE} are the charge transfer resistance and the double layer capacitance at the electrolyte/counter electrode interface and Z_d is the diffusion impedance in the electrolyte.[25] A high accuracy in the fitting was found, as observed in Fig. 5a. The fitting was accompanied by spectra simulation in order to properly identify in the impedance spectrum the different processes occurring in the cell. It was found that the use of a constant phase element instead of a pure capacitor to describe the Cathode 2 capacitance was critical to obtain a good spectra fitting. The constant phase element ideal factor was found to lie within the 0.8–1.0 range. The relatively high non-ideality of the cathode/electrolyte interface was attributed to the porous nature of the PEDOT film.

The electrocatalytic activity of the cathode can be analysed by measuring the impedance response of the complete cells. The semicircle occurring at high frequency (left side of the spectrum) is attributed to charge transfer processes in the cathode/electrolyte interface. This feature appears at similar frequencies with both types of cathodes (Pt@FTO: 2×10^3 Hz, Cathode 2: 1×10^3 Hz). The results for the series resistance (R_s), charge transfer resistance in the cathode (R_{CE}) and cathode capacitance (C_{CE}) at an applied bias of 0.7 V obtained by fitting the spectra to the equivalent circuit in Fig. 5b are summarized in Table 2. It is worth highlighting two simplifications which are assumed when comparing both types of cathodes. On the one hand, the Nernst diffusion impedance in pores for Cathode 2 is neglected.[26] On the other hand, the parameters are normalized to the geometric electrode area. However, a proper comparison of the electrocatalytic activity of Cathode 2 should take into account the total surface area of the cathode (obtained by BET experiments).[27]

The main contributions to R_s are given by the contacts, the conducting glass, charge transfer at the counter electrode and electrolyte diffusion resistances.[25] Series resistance is quite similar for both types of cathodes (Table 2), which indicates that Cathode 2 (PEDOT) does not introduce an additional series resistance loss.

The capacitance of the PEDOT cathode is higher than for Pt, as expected from the higher surface area of the former. Another plausible reason is the high charge retaining capability observed in conducting polymers. As pointed out by Ellis *et al.* PEDOT electrodes show pseudo-capacitive charging due to redox reactions, which will result in a higher capacity even for a flat PEDOT electrode.[28] As expected from measurements of the limiting current which yielded a similar response for both types of cathodes (Fig. 2), the charge transfer resistance in the cathode is comparable in both cases (Table 2).

Table 1 Photovoltaic properties of two cathodes, Pt@TCO and Cathode 2

Device	J_{sc} (mA cm$^{-2)}$	V_{oc} (mV)	FF	PCE
FTO/TiO_2/dye/electrolyte/Pt@FTO	13.4	802	63.8	6.9
Pt@FTO (average ± s.d.)[a]	12.4 ± 1.8	795.7 ± 12.7	64.9 ± 1.8	6.4 ± 0.8
FTO/TiO_2/dye/electrolyte/Cathode 2	13.4	790	66.1	7.0
Cathode 2 (average ± s.d.)[a]	12.6 ± 0.7	767 ± 20	64.8 ± 1.1	6.3 ± 0.6

[a] The average and standard deviation (s.d) values of 3 identically fabricated devices.

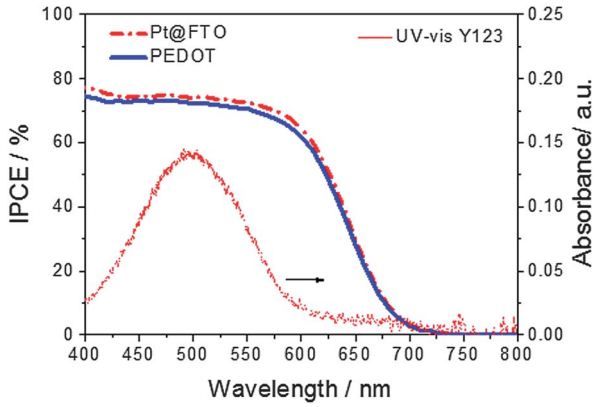

Fig. 4 IPCE for DSSCs fabricated with Cathode 2 (PEDOT) and a Pt@FTO cathode using the cobalt redox shuttle. UV-vis spectrum in solution of the sensitizer **Y123** used (secondary *Y*-axis).

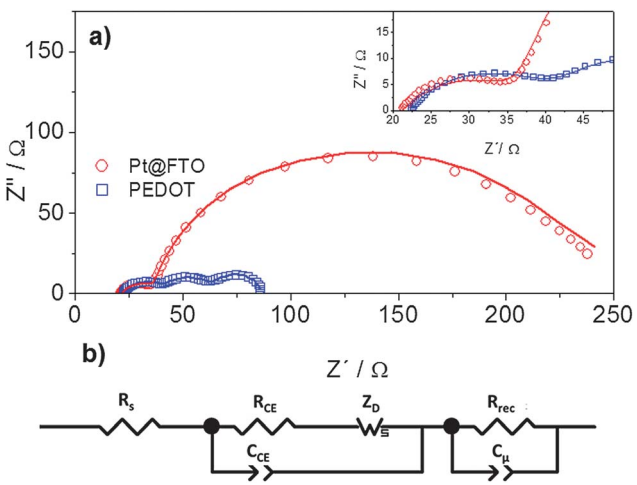

Fig. 5 (a) Nyquist plots at an applied bias of 0.7 V under illumination, including lines of best fit obtained from fitting the impedance spectra to the equivalent circuit shown in (b).

The semicircle at mid frequencies (middle part of the spectrum) is attributed to charge transfer at the oxide/electrolyte interface (recombination and electron accumulation in the oxide). In Fig. 6, the resistances (R_{rec}) and capacitances (C_μ) as a function of the applied potential at the same illumination level are plotted. Both quantities have an exponential behaviour with respect to the voltage, which is characteristic of the oxide/electrolyte interface.[29] In the past, the importance of correcting the IR drop in the potential scale was also emphasized.[30] However, taking into account a possible voltage drop due to series resistance, no significant modification is detected in the EIS data (data not shown). This is sort of expected as it could be inferred from the exponential behaviour of the R_{rec} with respect to the applied potential. The chemical capacitance is a measure of the density of states in titania. Fig. 6a illustrates that, at the same applied potential, the Cathode 2 (PEDOT)-based cell exhibits higher capacitance. As similar photoanodes and cell configuration except for the cathode are used in both cells, this difference in the capacitance of the TiO_2 films implies a downward shift of the band edge of the PEDOT-based DSSCs towards more positive potentials with respect to the Pt@FTO-based DSSCs. We assign the surface modification as a possible source for this, which arises due to the acidic nature of PEDOT:PSS compared with the platinized cathode, and can influence the band edge after diffusion to and adsorption on the TiO_2 surface. By comparing the charge transfer resistance (Fig. 6b), both kinds of cell exhibit relatively low values of the

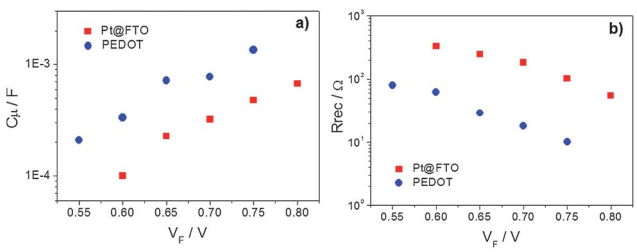

Fig. 6 Capacitance (a) and charge transfer resistance (b) at the oxide/electrolyte interface as a function of the applied voltage.

Table 2 Electrical parameters of the electrolyte/cathode interface obtained from EIS

Device	R_s (Ω cm^2)	R_{CE} (cathode/electrolyte) (Ω cm^2)	C_{CE} (cathode/electrolyte) (F cm^{-2})
FTO/TiO_2/dye/electrolyte/Pt@FTO	15.60	10.36	3.72×10^{-5}
FTO/TiO_2/dye/electrolyte/Cathode 2	16.09	13.51	1.08×10^{-3}

transfer coefficient β (around 0.2–3), which is the factor controlling the slope of the R_{rec}–potential curve.[30,31] Relatively low values of this coefficient have also been reported recently for TiO_2 cells sensitized with the **Y123** dye and cobalt-based electrolytes.[32] According to the results shown in Fig. 6b, at the same applied voltage the resistance to recombination is higher for Pt@FTO-based cells. However, a comparison of recombination rates can only be made if all the voltages are shifted to a scale in which the conduction band of titania would be at the same equivalent level for the different DSSCs.[29] Barea *et al.* emphasized that one should distinguish between the applied potential,[30] termed as the Fermi-level potential (V_F) as it reflects the rise of the Fermi level in TiO_2, and the common equivalent conduction band potential (V_{ecb}). In Fig. 7, lifetimes of the two types of cells are compared with respect to V_{ecb}, which is defined as:

$$V_{ecb} = V_F - \Delta E_c/q \quad (1)$$

In this equation, $\Delta E_c/q$ is the shift of the conduction band with respect to the sample taken as a reference. According to the capacitance data in Fig. 6a, the band displacement is around 100 mV for the PEDOT cell with respect to Pt@FTO.[33] Fig. 7 shows the electron lifetimes as a function of V_{ecb}, obtained from the capacitance and recombination resistance measured by impedance according to the expression:

$$\tau_n = R_{ct}C_{mu} \quad (2)$$

Using this representation, the lifetime directly reflects the rate of electron transfer. The lifetime is slightly longer in the case of the Pt@FTO cell (0.04 s at 0.75 V for platinum cells and 0.02 s at the same potential for PEDOT cells).

As shown in Fig. 3 and Table 1, the overall performance of the cell at steady state and under AM 1.5 illumination is very similar for both Pt-based and PEDOT-based cells. In spite of the slightly longer lifetime for the Pt-based cell, a difference of only 10 mV was found between both V_{oc} values. As discussed in the following section, the small difference in the lifetime does not lead to a significant effect on the photovoltage. It should be noted that it is the lifetime which determines the V_{oc} at 1 sun. The similar series resistance (Table 2), together with the similar slope of R_{rec} with respect to the applied potential as shown in Fig. 6b (β coefficient), explains the similar FF obtained for both cells.[34]

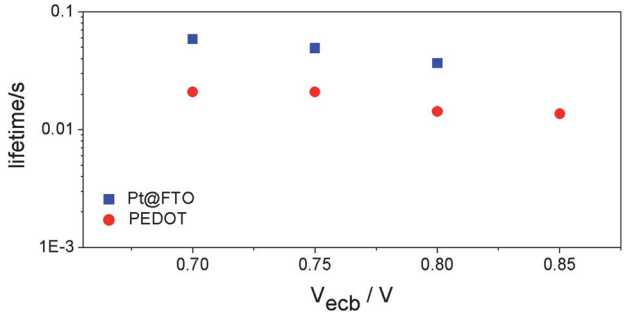

Fig. 7 Lifetime as a function of V_{ecb}.

2.4 Modelling

To gain further insight and understanding regarding the performance of the devices and the role of the recombination kinetics, we have solved the continuity equation for electrons in the active TiO_2 layer. This equation reads as[35,36]

$$\frac{\partial n(x,t)}{\partial t} = G(x) + \frac{\partial}{\partial x}\left(D(n)\frac{\partial n(x,t)}{\partial x}\right) - k_R(n)n(x,t) \quad (3)$$

where $n(x,t)$ is the total density of electrons in the film as a function of distance to the front contact (x) and time t, and $G(x)$ is an electron generation profile that involves the solar irradiance, the dye absorption spectrum, the quantum yield of electron injection and the dye loading in the film. It is worth mentioning that the modelling of the DSSCs can also be made in terms of a constant D and k_R coupled to trapping/detrapping terms. However, in the steady-state, both alternatives lead to the same I–V curve.[36] The continuity equation is solved for a density dependent diffusion coefficient $D(n)$ and a pseudo first order kinetic recombination constant $k_R(n)$ given by[37]

$$k_R(n(x)) = k_R^0 e^{((\beta - \alpha)qV_F/k_BT)} \quad (4)$$

where k_B is the Boltzmann constant and T the absolute temperature. The numerical solution of the continuity equation makes it possible to obtain the photocurrent from the gradient of the total density at $x = 0$ at a given value of the voltage V_F. In the calculation $G(x)$ is estimated from the dye spectrum and adjusted to reproduce the experimental short circuit photocurrent. In turn, k_R^0 is adjusted to reproduce the experimental photovoltage at open circuit.[35,36] This is achieved by imposing that the photocurrent is zero at $V_F = V_{oc}$. The parameters α and β are commonly taken from measurements of chemical capacitance and recombination resistance *versus* voltage. In this case, we have used $\alpha = 0.2$ and $\beta = 0.3$, as inferred from the impedance measurements in Fig. 6. For the Pt cell, the generation term was adjusted to give a short circuit photocurrent of ~13.4 mA cm^{-2} and k_R^0 was adjusted to yield V_{oc} = 800 mV. According to the lifetime data in Fig. 7, the recombination rate is approximately twice as large for the PEDOT cell. We have multiplied the recombination constant k_R^0 by a factor of two, and obtained a theoretical value of 746 mV for V_{oc}. Therefore doubling the recombination rate while keeping the same generation rate reduces the open circuit photovoltage by ~50 mV. Repeating the calculation but with $\alpha = 0.2$ and $\beta = 0.7$ (which is a more standard value of the recombination coefficient), the theoretical reduction in V_{oc} is ~25 mV. This is a relatively small variation, which justifies the similar V_{oc} for the two cells, in spite of the different impedance response. In fact, it has been reported[4] that a 2-fold increase in the recombination rate results in a decrease of 20–30 mV in the open circuit potential. The negligible impact on V_{oc}, together with the similar voltage dependence of the recombination resistance, and the closeness of the series and cathode resistances, explains the similitude between the I–V curves of the Pt and PEDOT cells.

3. Experimental section

3.1 Preparation of the counter electrodes

Metal grid electrodes (flextrodes), *i.e.* an Ag grid deposited on PEDOT flexible substrates, were kindly received from F. C. Krebs.[21] In short, a honeycomb structured Ag grid was flexographically printed followed by rotary-screen printing of PEDOT:PSS onto a flexible plastic substrate. To further increase the conductivity and to lower the sheet resistance, another layer of PEDOT was spin-coated on top of it. The coating was made using a formulation of PEDOT:PSS (PH1000) with 5 wt% of ethylene glycol at a speed of 2000 rpm for 30 s. In the text, the as-supplied electrode is defined as Cathode 1, while the electrode with an additional layer of spin-coated PEDOT is referred to as Cathode 2. The spin-coated films were then annealed at 120 °C on a hot plate for 15 minutes under laboratory conditions. The platinized cathode was prepared by spreading 20 μL of Platisol (Solaronix) over the FTO substrates (TEC8) and subsequent annealing at 390 °C for 20 min.

3.2 Cell fabrication

For optimized cell efficiencies, devices were made using 13 μm thick films consisting of a 9 μm layer of 20 nm TiO_2 nanoparticles (Dyesol© paste) and a 4 μm layer of 400 nm TiO_2 particles (scattering layer). Prior to the deposition of the TiO_2 paste, the conducting glass substrates (TEC15) were immersed in a solution of $TiCl_4$ (40 mM) for 30 minutes at 70 °C and then dried. A screen printing technique was employed to obtain reproducible results for the deposition of TiO_2 onto a conducting glass substrate. The TiO_2 electrodes were then gradually heated under airflow at 325 °C for 5 min, 375 °C for 5 min, 450 °C for 15 min and 500 °C for 15 min. Finally, the electrodes were heated again at 500 °C for 30 min and cooled to 80 °C before dye adsorption. The DSSC active area was 0.28 cm^2. The electrodes were immersed and kept for 15 hours at room temperature in a solution containing 0.1 mM of dye coded **Y123**: 3-{6-{4-[bis(2,4-dihexyloxybiphenyl-4-yl)amino-]phenyl}-4,4-dihexyl-cyclopenta-[2,1-b:3,4-b2]dithiphene-2-yl}-2-cyanoacrylic acid, and 5 mM of chenodeoxycholic acid in a 50/50 (v/v) mixture of acetonitrile and *tert*-butanol. The sensitized electrodes were then rinsed with the same mixture of solvents and dried in air. Finally, the working and counter electrodes were sandwiched together using a thin thermoplastic (Surlyn) frame that melts at 100 °C. In order to provide more mechanical support during measurements, a microslide glass plate was attached to the flexible cathode. The cells were filled with a cobalt-based electrolyte (0.2 M $Co(byp)_3(PF_6)_2$, 0.02 M $Co(byp)_3(PF_6)_3$, 0.5 M 4-*tert*-butylpiridine and 0.1 M $LiClO_4$ in acetonitrile) through a previously made hole in the rear side of the cathode. Finally, the hole was sealed with a thermoplastic polymer and a glass cover slide. The electrochemical performance of the PEDOT films was studied using a two-electrode cell (blank cell) consisting of one Pt@FTO electrode and one Cathode 2 (PEDOT electrode), sandwiched together and sealed with Surlyn. They were then filled with the cobalt redox shuttle used in the DSSC fabrication. Similar cells but with two platinum-based electrodes were fabricated for comparison purposes.

3.3 Characterization

The devices were characterized using a solar simulator with an AM 1.5 G filter (ABET). The light intensity was calibrated to the standard value of 1 sun (100 mW cm^{-2}) using a reference solar cell with temperature output (Oriel, 91150). The current–voltage characteristics were determined by applying an external potential bias to the cell and measuring the photocurrent using an Autolab/PGSTAT302N potentiostat. A mask covering the non-active parts of the cells was used when measuring the *I–V* characteristics. Electrochemical Impedance Spectroscopy (EIS) was utilized to study charge-transfer processes in the devices. Impedance measurements were carried out under varying bias potential (in the range between 0.55 V and 0.8 V) and under illumination. The illumination for the small perturbation (frequency response) technique was provided by a 540 nm light emitting diode (LUXEON) over a wide range of DC light intensities. A response analyzer module (PGSTAT302N/FRA2, Autolab) was utilized to analyze the frequency response of the devices. A 10 mV perturbation in the 10^{-2} to 10^5 Hz range was applied to obtain the spectra. In all cases, the samples were illuminated from the dye-coated TiO_2 electrode side. The NOVA 1.7 software was used to generate and treat the EIS data. ZView equivalent circuit modelling software (Scribner) was used to fit the EIS spectra. For the blank cells, EIS was carried out in the dark at different potentials and cyclic voltammograms (CV) were recorded between 1 V and −1 V at a scan rate of 20 mV s^{-1}. Incident photon-to-electron conversion efficiencies (IPCE) were measured by means of a 0.2 m monochromator (McPherson). The light intensity was determined as a function of the wavelength using a calibrated silicon photodiode (PH-100 Si, GENTECE).

4. Conclusion

We have demonstrated a highly efficient, flexible, and low-cost (Pt- and TCO-free) cathode for dye sensitized solar cells. The cathodes were prepared using a formulation of highly conductive poly(3,4-ethylenedioxythiophene) (PEDOT) and Ag metal grids on flexible substrates. The charge transfer resistance was further minimized with an additional spin-coated layer of highly conducting PEDOT:PSS. Impedance results show that the use of the new cathode formulation has not introduced any significant modifications in the series and cathode resistances of the solar cell. Furthermore, although the recombination resistance was altered with respect to the reference Pt cell, this variation was found to have little impact on the open circuit potential. As a mark, the performance of the solar cell made with a PEDOT counter electrode was found to match that of the reference Pt cell. We believe that these counter electrodes can easily be integrated into DSSCs for further market penetration and scale up processes. The PCE in these plastic cathodes is one of the best (7%) and it is comparable with the value of the conventional platinized cathodes (6.9%) under similar device architecture and conditions. Modelling experiments confirm the negligible influence on the *I–V* curve from the modification of the recombination resistance for the PEDOT cells observed by

EIS. The low series resistance of the PEDOT-based cathode points towards its similar electrical properties to platinized cathodes. To conclude, the present report puts forward a non-toxic, facile, and cost effective process for mass production of cathodes for DSSCs using a cobalt redox shuttle.

Acknowledgements

The authors thank Michael Grätzel and Manuel Doblaré Castellano profusely for the fruitful discussions and support.

Notes and references

1 S. Chu and A. Majumdar, *Nature*, 2012, **488**, 294.
2 B. O'Regan and M. Grätzel, *Nature*, 1991, **353**, 737.
3 A. Yella, H.-W. Lee, H. N. Tsao, C. Yi, A. K. Chandiran, M. K. Nazeeruddin, E. W.-G. Diau, C.-Y. Yeh, S. M. Zakeeruddin and M. Grätzel, *Science*, 2011, **334**, 629.
4 S. Ahmad, E. Guillen, L. Kavan, M. Grätzel and M. K. Nazeeruddin, *Energy Environ. Sci.*, 2013, **6**, 3439.
5 J.-H. Yum, E. Baranoff, F. Kessler, T. Moehl, S. Ahmad, T. Bessho, A. Marchioro, E. Ghadiri, J.-E. Moser, C. Yi, M. K. Nazeeruddin and M. Grätzel, *Nat. Commun.*, 2012, **3**, 631.
6 S. M. Feldt, E. A. Gibson, E. Gabrielsson, L. Sun, G. Boschloo and A. Hagfeldt, *J. Am. Chem. Soc.*, 2010, **132**, 16714.
7 J. Burschka, V. Brault, S. Ahmad, L. Breau, M. K. Nazeeruddin, B. Marsan, S. M. Zakeeruddin and M. Grätzel, *Energy Environ. Sci.*, 2012, **5**, 6089.
8 B. E. Hardin, H. J. Snaith and M. D. McGehee, *Nat. Photonics*, 2012, **6**, 162.
9 S. Ahmad, E. Dell'Orto, J.-H. Yum, F. Kessler, M. K. Nazeeruddin and M. Grätzel, *Chem. Commun.*, 2012, **48**, 9714; M. Biancardo, K. West and F. C. Krebs, *J. Photochem. Photobiol., A*, 2007, **187**, 395.
10 G. Y. Margulis, M. G. Christoforo, D. Lam, Z. M. Beiley, A. R. Bowring, C. D. Bailie, A. Salleo and M. D. McGehee, *Adv. Energy Mater.*, 2013, **3**, 1657.
11 Y. Fu, Z. Lv, S. Hou, H. Wu, D. Wang, C. Zhang and D. Zou, *Adv. Energy Mater.*, 2012, **2**, 37.
12 Y. Galagan, B. Zimmermann, E. W. C. Coenen, M. Jørgensen, D. M. Tanenbaum, F. C. Krebs, H. Gorter, S. Sabik, L. H. Slooff, S. C. Veenstra, J. M. Kroon and R. Andriessen, *Adv. Energy Mater.*, 2012, **2**, 103.
13 S. Yun, H. Zhang, H. Pu, J. Chen, A. Hagfeldt and T. Ma, *Adv. Energy Mater.*, 2013, **3**, 1407.
14 S. Ahmad, J.-H. Yum, Z. Xianxi, M. Grätzel, H.-J. Butt and M. K. Nazeeruddin, *J. Mater. Chem.*, 2010, **20**, 1654.
15 J. Kwon, V. Ganapathy, Y. H. Kim, K.-D. Song, H.-G. Park, Y. Jun, P. J. Yoo and J. H. Park, *Nanoscale*, 2013, **5**, 7838.
16 R. Trevisan, M. Döbbelin, P. P. Boix, E. M. Barea, R. Tena-Zaera, I. Mora-Seró and J. Bisquert, *Adv. Energy Mater.*, 2011, **1**, 781.
17 T. H. Lee, K. Do, Y. W. Lee, S. S. Jeon, C. Kim, J. Ko and S. S. Im, *J. Mater. Chem.*, 2012, **22**, 21624.
18 J. M. Pringle, V. Armel and D. R. MacFarlane, *Chem. Commun.*, 2010, **46**, 5367.
19 K. S. Lee, H. K. Lee, D. H. Wang, N. G. Park, J. Y. Lee, O. O. Park and J. H. Park, *Chem. Commun.*, 2010, **46**, 4505.
20 D. Angmo and F. C. Krebs, *J. Appl. Polym. Sci.*, 2013, **129**, 1–14.
21 M. Hosel, R. R. Sondergaard, M. Jorgensen and F. C. Krebs, *Energy Technol.*, 2013, **1**, 102–107.
22 T. T. Larsen-Olsen, R. R. Sondergaard, K. Norrman, M. Jorgensen and F. C. Krebs, *Energy Environ. Sci.*, 2012, **5**, 9467–9471.
23 S. Ahmad, T. Bessho, F. Kessler, E. Baranoff, J. Frey, C. Yi, M. Grätzel and M. K. Nazeeruddin, *Phys. Chem. Chem. Phys.*, 2012, **14**, 10631.
24 S. Ahmad, J.-H. Yum, H.-J. Butt, M. K. Nazeeruddin and M. Grätzel, *ChemPhysChem*, 2010, **11**, 2814.
25 F. Fabregat-Santiago, G. García-Belmonte, I. Mora-Seró and J. Bisquert, *Phys. Chem. Chem. Phys.*, 2011, **13**, 9083.
26 J. D. Roy-Mayhew, D. J. Bozym, C. Punckt and A. Aksay, *ACS Nano*, 2010, **4**, 6203.
27 T. N. Murakami and M. Grätzel, *Inorg. Chim. Acta*, 2008, **361**, 572.
28 H. Ellis, N. Vlachopoulos, L. Häggman, C. Perruchot, M. Jouini, G. Boschloo and A. Hagfeldt, *Electrochim. Acta*, 2013, **107**, 45.
29 F. Fabregat-Santiago, J. Bisquert, G. Garcia-Belmonte, G. Boschloo and A. Hagfeldt, *Sol. Energy Mater. Sol. Cells*, 2005, **87**, 117.
30 E. M. Barea, C. Zafer, B. Gultekin, B. Aydin, S. Koyuncu, S. Icli, F. F. Santiago and J. Bisquert, *J. Phys. Chem. C*, 2010, **114**, 19840.
31 J. Bisquert, F. Fabregat-Santiago, I. Mora-Seró, G. García-Belmonte and S. Giménez, *J. Phys. Chem. C*, 2009, **113**, 17278.
32 Y. Liu, J. R. Jennings, S. M. Zakeeruddin, M. Grätzel and Q. Wang, *J. Am. Chem. Soc.*, 2013, **135**, 3939.
33 V. González-Pedro, X. Xu, I. Mora-Seró and J. Bisquert, *ACS Nano*, 2010, **4**, 5783.
34 J. Bisquert and I. Mora-Seró, *J. Phys. Chem. Lett.*, 2010, **1**, 450.
35 E. Guillén, L. M. Peter and J. A. Anta, *J. Phys. Chem. C*, 2011, **115**, 22622.
36 J. A. Anta, J. Idigoras, E. Guillén, J. Villanueva-Cab, H. J. Mandujano-Ramírez, G. Oskam, L. Pelleja and E. Palomares, *Phys. Chem. Chem. Phys.*, 2012, **14**, 10285.
37 M. Ansari-Rad, J. A. Anta and J. Bisquert, *J. Phys. Chem. C*, 2013, **117**, 16275.